Journal of Catalysis 281 (2011) 63–75

Contents lists available at ScienceDirect

Journal of Catalysis

journal homepage: www.elsevier.com/locate/jcat

Theoretical study of 1,3-cyclohexadiene dehydrogenation on Pt (1 1 1), Pt_3Sn/Pt (1 1 1), and Pt_2Sn/Pt (1 1 1) surfaces

Hong-Yan Ma, Gui-Chang Wang *

Department of Chemistry and the Center of Theoretical Chemistry, Nankai University, Tianjin 300071, PR China

ARTICLE INFO

Article history:
Received 24 November 2010
Revised 9 March 2011
Accepted 3 April 2011
Available online 10 May 2011

Keywords:
1,3-Cyclohexadiene
Pt–Sn alloy
Adsorption
Dehydrogenation
DFT calculations

ABSTRACT

The 1,3-cyclohexadiene dehydrogenation to phenyl on the Pt (1 1 1), Pt_3Sn/Pt (1 1 1), and Pt_2Sn/Pt (1 1 1) surfaces has been studied using density functional theory calculation. The results show that the adsorption energies of 1,3-cyclohexadiene and other intermediates decrease with the increasing concentration of Sn. The addition of Sn weakens the interaction between the adsorbate and the alloys. The barriers are 0.62, 0.72, and 0.75 eV for the first and 0.87, 0.51, and 0.32 eV for the second step on the Pt (1 1 1), Pt_3Sn/Pt (1 1 1), and Pt_2Sn/Pt (1 1 1), respectively, for the dehydrogenation of the 1,3-cyclohexadiene. The third dehydrogenation step is the rate determining step (rds) with the barriers of 1.49, 1.75, and 1.90 eV on the Pt (1 1 1), Pt_3Sn/Pt (1 1 1), and Pt_2Sn/Pt (1 1 1), respectively. The existence of the Sn facilitates the first two dehydrogenation steps that produce benzene and prohibits further dehydrogenation of benzene, thus increases the selectivity of the dehydrogenation of 1,3-cyclohexadiene to gas benzene.

1. Introduction

The dehydrogenation of cyclohexadiene to benzene over Pt catalysts has been widely studied both experimentally and theoretically [1–7]. Pettiette-Hall et al. [1] observed substantial amount of benzene at low coverage of 1,3-cyclohexadiene at 115 K on the Pt (1 1 1) using laser-induced thermal desorption (LITD) and Fourier transform mass spectrometry (FTMS), indicating the barrier of cyclohexadiene dehydrogenation to benzene was very low. Later, Hugenschmidt et al. [2] found that the dehydrogenation of 1,3- and 1,4-cyclohexadiene occurred at about 230–260 K with an activation energy of 0.61 ± 0.09 eV on the Pt (1 1 1). Saeys et al. [4] studied the hydrogenation of benzene on the Pt (1 1 1) using density functional theoretical (DFT) methods, and the calculated barrier of 1,3-cyclohexadiene dehydrogenation was 0.55–0.82 eV. Then, they found four possible adsorption modes for 1,3-cyclohexadiene on the Pt (1 1 1) applying ab initio density functional theory [5]. In the meantime, Morin et al. [6] investigated the adsorption of the species involved in benzene hydrogenation to cyclohexene, using a first principles density functional theory and a periodical slab model.

Supported Pt–Sn bimetallic catalysts have been investigated widely [8–12], for they played an important role in selective dehydrogenation/hydrogenation reactions. Butadiene hydrogenation by coadsorbed hydrogen on the Pt–Sn surface alloys was observed to have 100% selectivity to liberate butene (C_4H_8), and no deeper hydrogenation occurred, when the technical of temperature-programmed desorption (TPD) and Auger electron spectroscopy (AES) were used [9]. And the addition of Sn led to a new hydrogenation reaction pathway compared with Pt (1 1 1) [9]. Recently, Vigné et al. [10] illuminated the origin of the high selectivity for the hydrogenation of 1,3-butadiene on the Pt_2Sn/Pt (1 1 1) surface with periodic DFT calculations. Peck and Koel [11] found the Pt–Sn surface alloys dramatically increased the selectivity of gas-phase benzene produced by 1,3-cyclohexadiene dehydrogenation, using AES, low-energy electron diffraction (LEED) and TPD.

In this study, we present our theoretical study of adsorption and reaction involved in 1,3-cyclohexadiene dehydrogenation to phenyl radical C_6H_5 on the Pt (1 1 1), Pt_3Sn/Pt (1 1 1), and Pt_2Sn/Pt (1 1 1) using periodic models. We attempt to identify: (1) the rules of adsorption for 1,3-cyclohexadiene and other species on the Pt (1 1 1) and Pt–Sn surface alloys as well as the influence of the Sn atom; (2) the mechanism of the dehydrogenation reactions; and (3) the reason for the excellent selectivity of the Pt_2Sn/Pt (1 1 1) surface alloy for gas-phase benzene production, by optimizing the structure, analyzing the electron structure, searching for the transition state (TS) and microkinetic modeling.

2. Computational details

The calculations have been performed by the Vienna ab initio simulation package (VASP) [13–15]. The projector-augment wave (PAW) [16] scheme and generalized gradient approximation (Perdew – PW 91) [17] were used to describe the electron–ion interaction and the exchange–correlation energy and potential.

* Corresponding author. Fax: +86 22 23502458.
E-mail address: wangguichang@nankai.edu.cn (G.-C. Wang).

0021-9517/$ - see front matter © 2011 Elsevier Inc. All rights reserved.
doi:10.1016/j.jcat.2011.04.002

The energy cutoff was set to be 400 eV. The surfaces were modeled by periodic four-layer slabs. Only the first layer of the catalysts contained Sn atoms with the stoichiometry of Pt_3Sn/Pt (1 1 1) for the (2×2) Pt_3Sn/Pt (1 1 1) and Pt_2Sn/Pt (1 1 1) for the $(\sqrt{3} \times \sqrt{3})$ R30° Pt_2Sn/Pt (1 1 1) structures, since the prepared alloys were monolayer alloys with the alloying atoms deposited on platinum [18]. Both the Pt (1 1 1) and the Pt_2Sn/Pt (1 1 1) were modeled by (3×3) (1/9 ML) super cell (Fig. 1A and B). The Pt_3Sn/Pt (1 1 1) surface alloy was modeled by (4×4) (1/16 ML) super cell (Fig. 1C). Considering the (4×4) super cell may be too large to model the Pt_3Sn/Pt (1 1 1) when compared with the (3×3) model of Pt (1 1 1) and the Pt_2Sn/Pt (1 1 1), we have also built the $(2\sqrt{3} \times 2\sqrt{3})$ R30° unit cell (1/12 ML) (Fig. 1D). In fact, the results based on the (4×4) cell are similar to that based on the $(2\sqrt{3} \times 2\sqrt{3})$ R30° cell, so we mainly use the (4×4) cell to model the Pt_3Sn/Pt (1 1 1) surface alloy in this work. One molecule was adsorbed per unit cell. The total energy has been calculated with a $5 \times 5 \times 1$ k-point grid. And the central slab and its periodic images have been separated by a vacuum space of 11.5 Å. Only the two uppermost metal layers and the adsorbed molecule were allowed to fully relax for the geometry optimization. The forces on all unconstrained atoms were less than 0.05 eV/Å after optimization. The saddle points were first searched by the nudged elastic band (NEB) [19] implemented in the VASP. Then, a quasi-Newton algorithm was used to refine the obtained approximate TS by minimizing residual forces below 0.03 eV/Å. Finally, the TS was identified by verifying the existence of one and only one normal mode associated with a pure imaginary frequency.

The nearest distance of the Pt atoms was frozen at the optimized value of 2.82 Å (experimentally 2.77 Å [20]) on Pt (1 1 1). The distance between adjacent Pt and Sn atom in the surface alloys was computed to be increased slightly to 2.86 Å, owing to the large covalent radius of Sn. This also led to the fact that Sn atoms were buckled out of the surface layer by 0.31 Å for the Pt_2Sn/Pt (1 1 1) and by 0.25 Å for the Pt_3Sn/Pt (1 1 1), in remarkable agreement with the experimental observations [21,22], which had major effect on the distortion of the molecule and the surface during adsorption (see Table 1). The unit cell had a net dipole due to the adsorption of molecules on one side of the slab only, and the total energy could be affected by a spurious electrostatic interaction between the slab and its periodic images. A dipole correction has been applied both on the energy and the potential in order to remove this effect. The adsorption energy has been obtained as the difference between the energy of the whole system and that of the sum of the bare slab and the isolated adsorbate.

A systematic notation has been used to describe the adsorption sites and molecule geometries. For example, fcc 1,4-di-σ-2,3-π, where fcc indicates the adsorption site, the integers label the carbon atoms in the molecule, while 'σ' denotes the interaction between only one carbon atom with one surface Pt atom and 'π' denotes the interaction between two consecutive carbon atoms with the same surface Pt atom.

3. Adsorption of the involved species

In this section, we first discuss the adsorption of 1,3-cyclohexadiene, cyclohexadienyl, benzene, C_6H_5, and H-atom on the Pt (1 1 1) and Pt–Sn surface alloys. Then, we try to find the rule of adsorption and the influence of Sn on the reactivity of the surface alloys by electronic structure analysis and decomposition of adsorption energy.

3.1. Adsorption of 1,3-cyclohexadiene

Three adsorption modes are considered for the adsorption of 1,3-cyclohexadiene on the Pt (1 1 1) surface. Table 1 illustrates the adsorption energies and detailed structural properties. Fig. 2A–C shows the top and side view of these adsorption modes to compare with the adsorption modes on the alloys. The most favored adsorption mode is fcc 1,4-di-σ-2,3-π with an adsorption energy of −1.53 eV. This value is in agreement with the adsorption energy of −1.48 eV proposed by Saeys et al. [5] and shows a discrepancy with the adsorption energy of −1.41 eV determined by Morin et al. [6] The bri 1,2-di-σ-3,4-π mode is slightly less preferred with a calculated adsorption energy of −1.45 eV. This value is similar to −1.42 eV provided by Morin et al. [6], but diverges from the value of −1.60 eV reported by Saeys et al. [5] who suggested this adsorption mode was the most favored. Besides, we notice the hcp di-π adsorption mode (Fig. 2C) with adsorption energy of −0.98 eV. In Morin et al. [6]'s study the adsorption energy of the di-π mode was −1.0 eV, but in Saeys et al. [5]'s study the hollow di-π adsorption mode was unstable, easily relaxing to other site. The

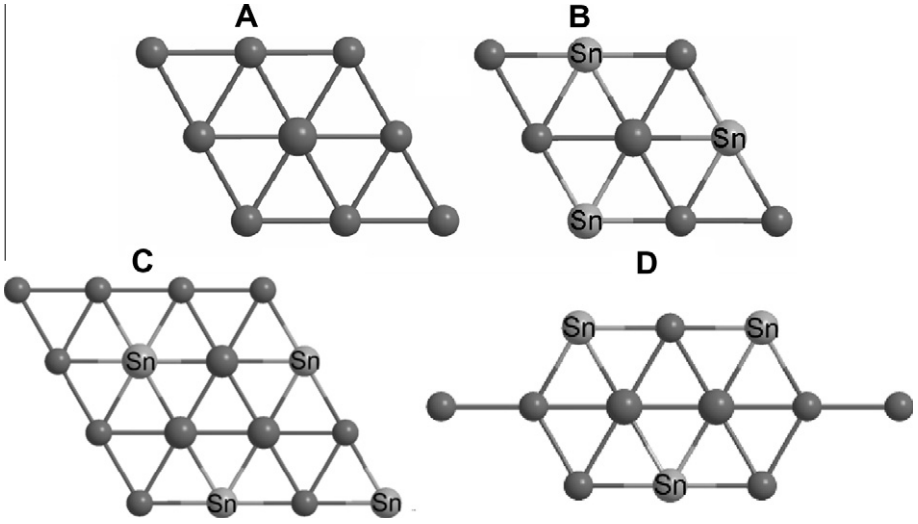

Fig. 1. Models used in the DFT calculations. (A and B) The (3×3) (1/9 ML) cell for the Pt (1 1 1) and Pt_2Sn/Pt (1 1 1). (C and D) The (4×4) (1/16 ML) and $(2\sqrt{3} \times 2\sqrt{3})$ R30° (1/12 ML) cells for the Pt_3Sn/Pt (1 1 1). Only the first layer of the models is shown, and the balls labeled as "Sn" represent Sn atoms, the other balls represent Pt atoms.

Table 1
Calculated thermodynamic data for 1,3-cyclohexadiene, cyclohexadienyl, benzene, and C_6H_5 adsorption on Pt (1 1 1), Pt_3Sn/Pt (1 1 1), Pt_2Sn/Pt (1 1 1) at the different high symmetry sites.

Species	Metal surface	Adsorption mode	E_{ads} (eV)	d_{C-C} (Å)	d_{C-M} (Å)	$E_{dist\ (mole)}$ (eV)	$E_{dist(surf.)}$ (eV)	E_{inter} (eV)	$\Delta\Phi$ (eV)
C_6H_8	Pt (1 1 1)	fcc1,4-di-σ-2,3-π	−1.53	1.50	2.46	2.58	0.21	−4.32	1.72
		bri 1,2-di-σ-3,4-π	−1.45	1.49	2.43	2.04	0.18	−3.67	1.81
		hcp di-π	−0.98	1.48	2.50	0.84	0.40	−2.22	1.92
	Pt_3Sn/Pt (1 1 1)	fcc 1,4-di-σ-2,3π	−0.89(−0.88)	1.50	2.55	2.72	0.60	−4.21	1.21
		hcp 1,2-di-σ	−0.67	1.48	2.95	1.36	0.46	−2.49	0.97
		fcc di-π	−0.54	1.48	2.67	0.93	0.79	−2.26	1.41
	Pt_2Sn/Pt (1 1 1)	fcc 1,2-di-σ	−0.40	1.48	2.87	1.42	0.46	−2.28	1.17
		bri 1,4-di-σ	−0.10	1.49	2.80	2.26	0.50	−2.86	1.16
		fcc di-π	−0.28	1.48	2.71	0.90	0.94	−2.12	1.91
C_6H_7	Pt (1 1 1)	hcp 1π3σ	−2.15	1.49	2.21	2.10	0.28	−4.53	1.81
		fcc 1π2σ	−2.10	1.47	2.33	1.23	0.29	−3.62	1.97
		bri 2π1σ	−2.08	1.47	2.28	0.97	0.21	−3.26	2.00
	Pt_3Sn/Pt (1 1 1)	fcc 2π1σ	−1.02(−1.00)	1.47	2.45	1.36	0.90	−3.28	1.37
		hcp 1π1σ	−1.00	1.45	2.70	0.77	0.56	−2.33	1.15
	Pt_2Sn/Pt (1 1 1)	fcc 1π1σ	−0.99	1.46	2.72	0.96	0.66	−2.61	1.73
		bri 1σ	−0.84	1.44	3.15	0.66	0.27	−1.77	1.25
C_6H_6	Pt (1 1 1)	bri 2π2σ	−0.80	1.46	2.13	1.52	0.25	−2.57	1.97
		fcc 3π	−0.47	1.44	2.19	0.83	0.27	−1.57	2.01
	Pt_3Sn/Pt (1 1 1)	bri	0.01(0.01)	1.40	3.33	0.00	0.00	0.01	0.58
	Pt_2Sn/Pt (1 1 1)	fcc	0.06	1.40	3.33	0.00	0.00	0.06	0.83
C_6H_5	Pt (1 1 1)	top1σ	−2.33	1.40	3.46	0.12	0.09	−2.54	0.88
	Pt_3Sn/Pt (1 1 1)	top1σ	−2.21(−2.20)	1.40	3.75	0.13	0.21	−2.55	0.58
	Pt_2Sn/Pt (1 1 1)	top1σ	−1.42	1.40	3.40	0.18	0.18	−1.78	0.73
H	Pt (1 1 1)	hcp	−0.49	_	_	_	_	_	_
		bri	−0.45	_	_	_	_	_	_
		top	−0.44	_	_	_	_	_	_
		fcc	−0.43	_	_	_	_	_	_
	Pt_3Sn/Pt (1 1 1)	fcc	−0.47	_	_	_	_	_	_
		hcp	−0.37	_	_	_	_	_	_
		top	−0.36	_	_	_	_	_	_
	Pt_2Sn/Pt (1 1 1)	top	−0.35	_	_	_	_	_	_
		bri	−0.14	_	_	_	_	_	_

Note: $E_{ads} = E$ (coadsorbed system) − E (molecule isolated) − E (bare surface), and the zero of the energy scale is set to the bottom of the molecule gas-phase potential.
E_{dist} (mole): distortion energy for molecule. E_{dist} (surf.): distortion energy for metal surface.
E_{inter}: interaction energy between the molecule and the surface, $E_{inter} = E_{ads} - E_{dist}$(mole) − E_{dist}(surf.).
d_{C-C}: average C–C bond length. d_{C-M}: the distance between the C_6 ring center and the metal surface for both flat and vertically adsorbed spieces.
$\Delta\Phi$: change in work function between the bare metal surface and the coadsorbed system.
The values in brackets are calculated on the $(2\sqrt{3} \times 2\sqrt{3})$ R30° cell for Pt_3Sn/Pt (1 1 1), while the other values are calculated on the (4×4) cell for Pt_3Sn/Pt (1 1 1).

different model used by Saeys et al. (22-atom cluster model) may cause the discrepancy in the calculated adsorption energies.

The adsorption energy of 1,3-cyclohexadiene diminishes on the Pt–Sn alloys compared with that on the Pt (1 1 1) (see Table 1). For example, the di-σ-π adsorption mode is favored both on the Pt_3Sn/Pt (1 1 1) and Pt (1 1 1), but the corresponding adsorption energy on the Pt_3Sn/Pt (1 1 1) is less exothermic than that on the Pt (1 1 1) by a margin of 0.64 eV. The energy cost by the distortion and weak interaction between the molecule and the alloy surfaces account for the small adsorption energy on the Pt–Sn alloy [6,23]. Besides, there are no threefold hollow sites composed entirely of Pt atoms on the Pt_2Sn/Pt (1 1 1) on account of the high coverage of Sn (shown in Fig. 1). Thus, no di-σ/π adsorption mode is favored on the Pt_2Sn/Pt (1 1 1). However, the di-π adsorption mode is observed on both the Pt (1 1 1) and Pt–Sn surface alloys, as adopting this mode requires just two consecutive Pt atoms.

The adsorptions of butadiene [10], ethene [24], α-β-unsaturated aldehydes [21,25], acetaldehyde [26], cyclopentene [27], and cyclohexane [28] have been studied both experimentally and theoretically on the Pt (1 1 1) and Pt–Sn surface alloys. A large decrease in the adsorption energies was also observed on the alloys. The primary role of Sn was considered as an interferer weakening the adsorption on the alloys. Becker et al. [23] pointed out that decrease in the adsorption energy on the Pt–Sn alloys was mainly attributed to relaxation effects of the surfaces, by investigating the adsorption of two prototypical alkenes on the Pt (1 1 1) and Pt–Sn surface alloys.

3.2. Adsorption of cyclohexadienyl

Three stable adsorption structures for cyclohexadienyl have been found on the Pt (1 1 1) (Fig. 3A–C). The adsorption energies for the most and the second stable modes are −2.15 and −2.10 eV, similar to the values of −2.20, −2.17 eV reported by Morin et al. [6]. Moreover, the cyclohexadienyl prefers to be adsorbed at the fcc-site on the Pt–Sn alloys (see Fig. 3D–G), and the corresponding adsorption energies are −1.02 and −0.99 eV on the Pt_3Sn/Pt (1 1 1) and Pt_2Sn/Pt (1 1 1), respectively.

3.3. Adsorption of benzene

The adsorption of the benzene molecule on the Pt surface has already been extensively studied by theoretical calculations. The most stable structure is the bri 2π2σ (see Fig. 4A) with the adsorption energy of −0.80 eV on the Pt (1 1 1). The less favored structure is the fcc 3π with the adsorption energy of −0.47 eV. However, the calculated adsorption energies for the above two cases were −0.90 and −0.67 eV in Morin et al. [6]'s work. Benzene is chemically adsorbed on the Pt (1 1 1), whereas physisorbed on the Pt–Sn surface alloys [28]. Thus, the interaction between the benzene and the Pt–Sn alloys is weak. This is in agreement with the average distance between the molecule and the metal surface: 2.13 Å on the Pt (1 1 1), 3.33 Å on the Pt–Sn alloys. The shorter the distance, the stronger interaction will be. Benzene desorbs from Pt–Sn surface alloys easily. This coincides with Peck and Koel [11]'s results that

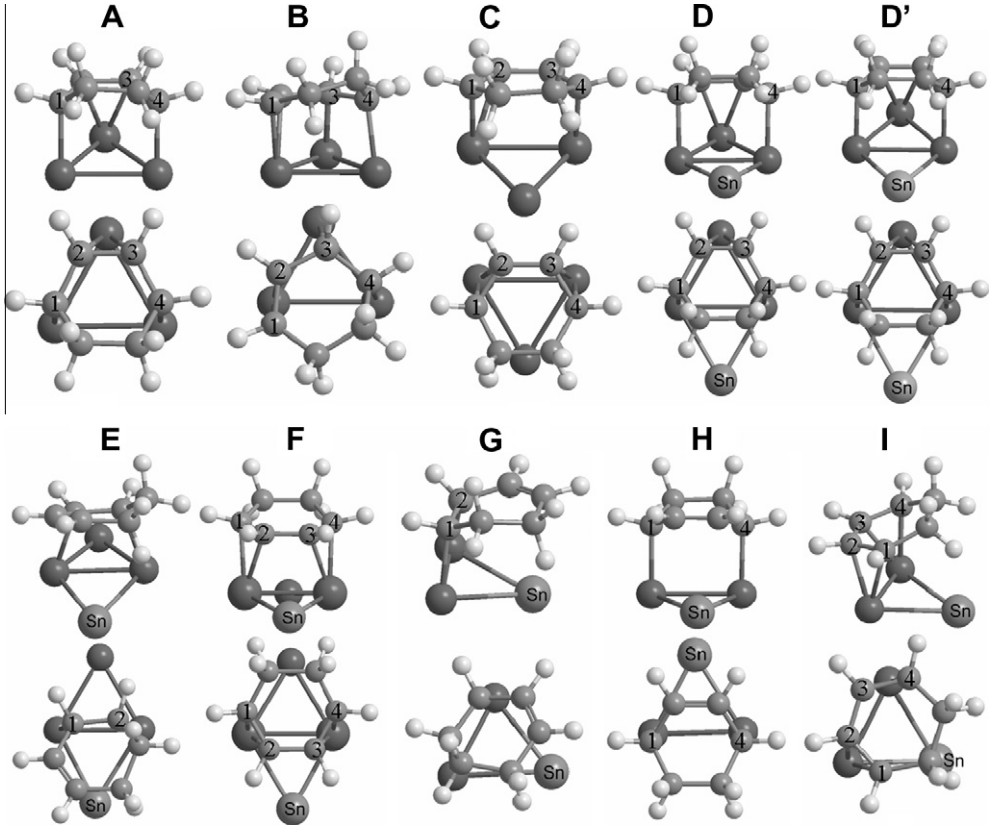

Fig. 2. Top and side view of 1,3-cyclohexadiene adsorbed at different sites on Pt (1 1 1)(A-C), Pt_3Sn/Pt (1 1 1) (D–F), and Pt_2Sn/Pt (1 1 1) (G–I): (A) fcc 1,4-di-σ/2,3-π; (B) bri 1,2-di-σ/3,4-π; (C) hcp di-π; (D) fcc 1,4-di-σ/2,3-π ((4×4) cell); (D′) fcc 1,4-di-σ/2,3-π ($(2\sqrt{3} \times 2\sqrt{3})$ cell); (E) hcp 1,2-di-σ ((4×4) cell); (F) fcc di-π ((4×4) cell); (G) fcc 1,2-di-σ; (H) bri 1,4-di-σ; (I) fcc di-π. Carbon atom numbers (1, 2, 3, and 4) are displayed for clarity.

benzene desorption occurred at 280 and 230 K on the Pt_3Sn/Pt (1 1 1) and Pt_2Sn/Pt (1 1 1) alloy surface, at the coverage produced by a dose of 0.55 L 1,3-cyclohexadiene (approximately 0.25 monolayer), while no benzene desorption occurred on the Pt (1 1 1) surface.

3.4. Adsorption of phenyl

Phenyl C_6H_5 prefers to vertically adsorb on the top of one surface Pt atom on both Pt (1 1 1) and Pt–Sn surfaces (Fig. 5A–C). In this way, all the C and H atoms in the molecule are nearly in the same plane, resulting in small distortion of the molecule and the support. The absolute value of the adsorption energy of C_6H_5 decreases in the order of Pt (1 1 1) > Pt_3Sn/Pt (1 1 1) > Pt_2Sn/Pt (1 1 1). Besides, the calculated adsorption energy of Phenyl on the Pt (1 1 1) is less exothermic than Gao et al.' results [29] (−2.33 eV is our result whereas −2.78 eV is Gao et al.'s). The different basis sets and *k*-point grid may cause the difference in adsorption energy (Gaussian-basis sets and $4 \times 4 \times 1$ *k*-point used by Gao et al., whereas we used the plan-wave basis sets and $5 \times 5 \times 1$ *k*-points).

3.5. Adsorption of hydrogen atom

The adsorption energy of hydrogen has been calculated according to: $E_{ads} = E(H_{ads}) - 1/2E(H_{2\ gas}) - E(\text{bare surface})$, to be compared with literature data. Some theoretical studies [4,30,31] indicated that hydrogen atoms were adsorbed at the top-site on the Pt (1 1 1). But the favorite adsorption site is the hcp-site on the Pt (1 1 1) with the adsorption energy of −0.49 eV in our calculation. The calculated hydrogen adsorption energies of −0.45, −0.44, and −0.43 eV are corresponding to the bri-, top-, and fcc-sites on the Pt (1 1 1). And these results are within the range of −0.3 to −0.43 eV obtained from the experiments at low hydrogen coverage [32–34]. The difference of the hydrogen adsorption energy at different adsorption sites is less than 0.06 eV on the Pt (1 1 1). As a consequence, the hydrogen atom diffuses quickly across the Pt (1 1 1) surface [35,36]. The most favored site is the top-site for hydrogen on Pt_2Sn/Pt (1 1 1), and this is in agreement with the results of Vigné et al. [10]. Furthermore, the absolute value of the adsorption energy of hydrogen also decreases in the order of Pt (1 1 1) > Pt_3Sn/Pt (1 1 1) > Pt_2Sn/Pt (1 1 1).

3.6. Work function and projected density of state (PDOS) analysis

The surface work function (Φ) is the minimum energy required to extract one electron from the surface to the vacuum. It is obtained by subtracting the Fermi level (E_{fermi}) from the plane-averaged electrostatic potential normal to the surface of the system (E_{vacum}) [37]. Thus, the surface work function (Φ) is quite sensitive to the charge density distribution of the surface. The clean Pt (1 1 1), Pt_3Sn/Pt (1 1 1), and Pt_2Sn/Pt (1 1 1) surfaces exhibit their work function at 5.74, 5.36, and 5.26 eV, respectively, in good agreement with the corresponding experimental values of 5.80, 5.40, and 5.20 eV [38]. The calculated Φ of the clean surface follows a decreasing order of Pt (1 1 1) > Pt_3Sn/Pt (1 1 1) > Pt_2Sn/Pt (1 1 1). This sequence is the same as the adsorption energies for all the species we have discussed above. Moreover, after adsorption, the Φ of the Pt (1 1 1), Pt_3Sn/Pt (1 1 1), and Pt_2Sn/Pt (1 1 1) decreases sharply. And similar cases were also observed on other alloys surfaces [39,40], implying charge transferring from the molecule to the metal surface. It seems that there is no direction relationship

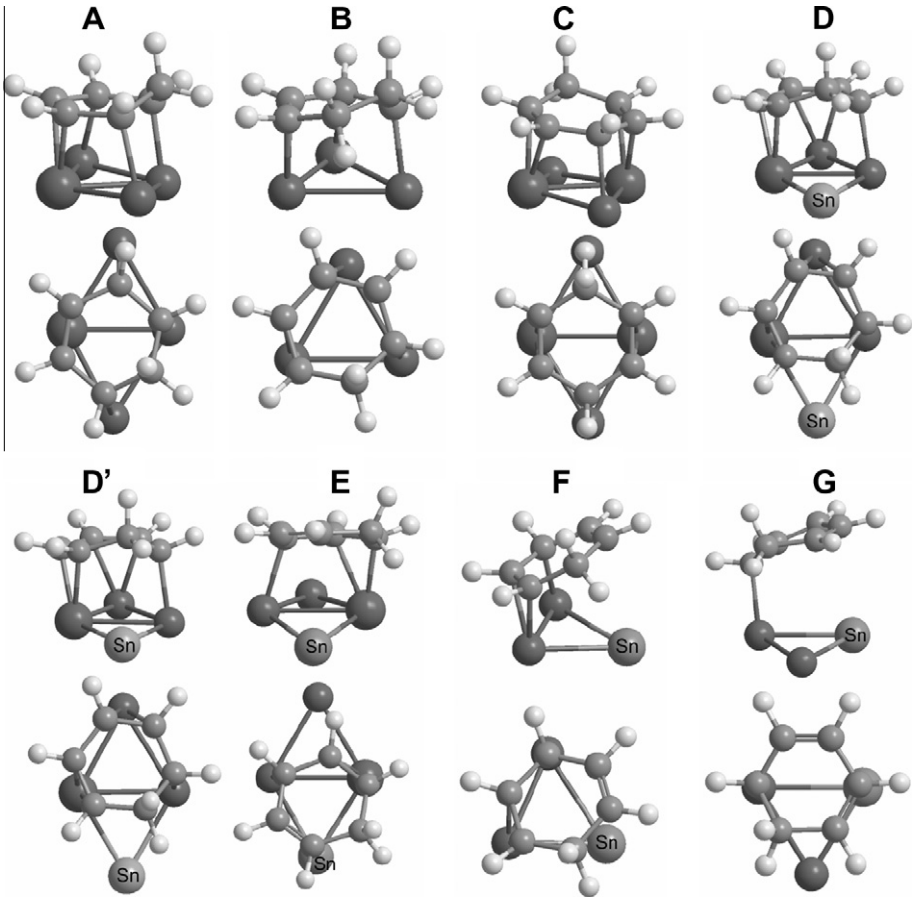

Fig. 3. Top and side view of cyclohexadienyl adsorbed at different sites on Pt (1 1 1) (A–C), Pt_3Sn/Pt (1 1 1) (D–E) and Pt_2Sn/Pt (1 1 1) (F–G): (A) hcp 1π3σ; (B) fcc 1π2σ; (C) bri 2π1σ; (D) fcc 2π1σ ((4 × 4) cell); (D′) fcc 2π1σ ((2√3 × 2√3) cell); (E) hcp 1π1σ ((4 × 4) cell); (F) fcc 1π1σ; (G) bri 1σ.

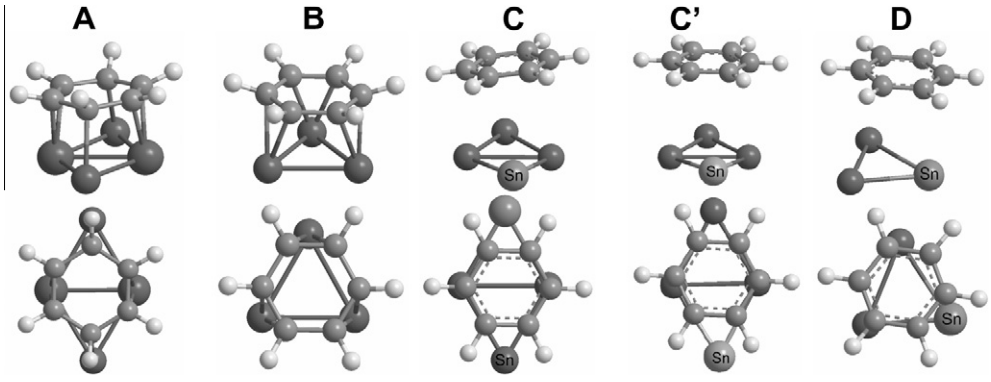

Fig. 4. Top and side view of benzene adsorbed at different sites on Pt (1 1 1) (A–B), Pt_3Sn/Pt (1 1 1) (C), and Pt_2Sn/Pt (1 1 1) (D). (A) bri 2π2σ; (B) fcc 3π; (C) bri ((4 × 4) cell); (C') bri ((2√3 × 2√3) cell); (D) fcc.

between the adsorption energy and the changes of the Φ (see Table 1). But the number of C–H bond that is formed between the molecule and the surface influences the reduction in the Φ. In general, the more C–Pt bonds in the adsorption mode, the larger curtailment of the Φ. For example, the Φ of the Pt_2Sn/Pt (1 1 1) surface is reduced by 1.91 eV after 1,3-cyclohexadiene adopts the fcc di-π mode (four C–Pt bonds in the di-π mode). While the Φ of the Pt_2Sn/Pt (1 1 1) surface is reduced by 1.17 eV after the molecule adopts the fcc 1,2-di-σ mode (two C–Pt bonds in the di-σ mode).

The position of the occupied d-band center (ε_d^c) relative to the Fermi level is an important surface parameter in determining the reactivity [41], which reflects the property of the local adsorption site of either the unperturbed metal surface or the variations in reactivity for metal overlayers and for different surface structures [42]. Many studies have shown that ε_d^c could be correlated with adsorption energies or activation energy barriers [43–45]. The d-band center (ε_d^c) is calculated by the formula [43]:

$$\varepsilon_d^c = \frac{\int_{-\infty}^{E_f} E\rho_d(E)dE}{\int_{-\infty}^{E_f} \rho_d(E)dE}$$

where ρ_d represents the density of states projected onto the d-band of metal atom and E_f is the Fermi level. Generally speaking, the closer the d-band center to the Fermi level, the more electrons at

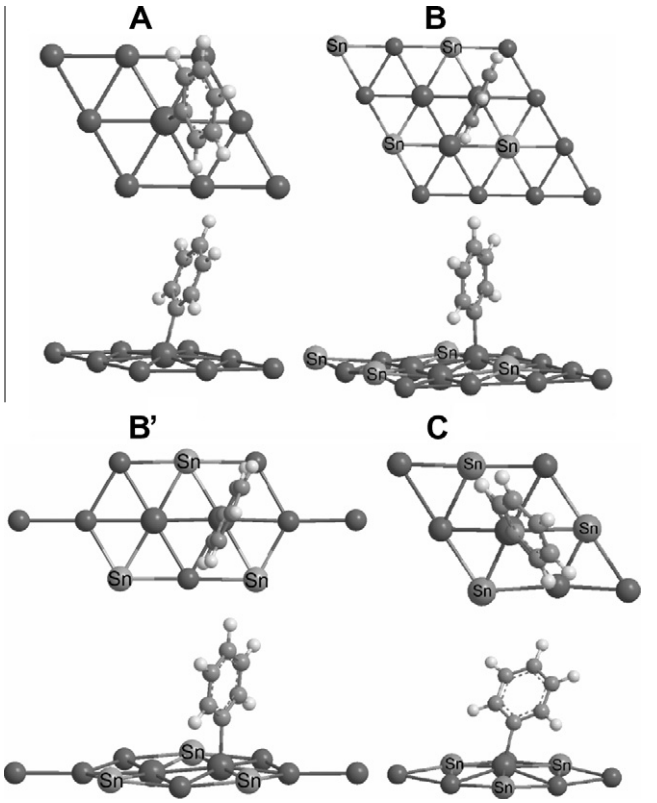

Fig. 5. Top and side view of phenyl adsorbed at different sites on Pt (1 1 1) (A), Pt_3Sn/Pt (1 1 1) (B), and Pt_2Sn/Pt (1 1 1) (C). (A) Top σ; (B) top σ((4 × 4) cell); (B′) top σ((2√3 × 2√3) cell); (C) top σ.

the Fermi lever, the higher reactivity the metal. Fig. 6A displays the PDOS plots of the metallic d-band for the Pt (1 1 1) and Pt–Sn surface alloys. The bandwidth increases from the Pt (1 1 1) to Pt_2Sn/Pt (1 1 1). And different shapes around the Fermi level (E_f) are observed: in the case of Pt (1 1 1), there is a large density of states just at E_f, which is smaller in the case of the Pt_3Sn/Pt (1 1 1) and almost disappears for the Pt_2Sn/Pt (1 1 1). Moreover, the position of the d-band center relevant to the corresponding Fermi level is calculated at −2.45, −2.61, and −2.63 eV, for the Pt (1 1 1), Pt_3Sn/Pt (1 1 1), and the Pt_2Sn/Pt (1 1 1), respectively. There is some difference between our values and the results from Delbecq and Vigné [46], but the conclusion is the same: the d-band center goes down when platinum is alloyed with Sn. Additional, the whole d-band center was also calculated in this work, and it was found that the d-band center is –1.95, –2.14, and –2.17 eV on Pt (1 1 1), Pt_3Sn/Pt (1 1 1) and Pt_2Sn/Pt (1 1 1), respectively, which has the same order as the occupied d-band center.

3.7. Decomposition of the adsorption energy

The adsorption energy can be decomposed into one term relating to the binding interaction to the metal (E_{inter}), and the other term (E_{dist}) relating to the distortion of the molecule and the metal as compared with its gas-phase state [6,47]. The two terms give opposite contributions. On the one hand, the distortions of the molecule and metal surface cause a destabilization; on the other hand, the interaction with the metal improves the stability of the system [48]. This can be expressed by an equation:

$$E_{ads} = E_{dist(molec)} + E_{dist(surf)} + E_{inter} \quad (1)$$

These terms are listed for 1,3-cyclohexadiene and other species on the Pt (1 1 1), Pt_3Sn/Pt (1 1 1), and Pt_2Sn/Pt (1 1 1) in Table 1. Generally speaking, the $E_{dist(molec)}$ for the flatly adsorbed species decreases in the order of Pt (1 1 1) > Pt_3Sn/Pt (1 1 1) > Pt_2Sn/Pt (1 1 1), except that the $E_{dist(molec)}$ of the 1,3-cyclohexdiene on the Pt_3Sn/Pt (1 1 1) is larger than that on the Pt (1 1 1). On the contrary, the $E_{dist(molec)}$ for the vertically adsorbed phenyl increases from the Pt (1 1 1) to Pt_2Sn/Pt (1 1 1). Furthermore, $E_{dist(molec)}$ can be correlated to the geometrical distortion and the energy gap between the highest occupied molecule orbital (HOMO) and the lowest unoccupied molecule orbital (LUMO) levels of the adsorbates [48,49]. The HOMO–LUMO gap decreases as distortion increases [48,49]. For example, the HOMO–LUMO gap of 1,3-cyclohexadiene in distorted geometry as di-π adsorption mode is 2.44, 2.30, and 2.40 eV (Fig. 6B) on the Pt (1 1 1), Pt_3Sn/Pt (1 1 1), and Pt_2Sn/Pt (1 1 1) surfaces, respectively. And the corresponding $E_{dist(molec)}$ is 0.84, 0.93 and 0.90 eV on the Pt (1 1 1), Pt_3Sn/Pt (1 1 1), and Pt_2Sn/Pt (1 1 1), respectively. The molecule distortion suggests a stabilization of vacant molecule orbitals and a destabilization of occupied orbitals. High distortion implies a better electronic interaction between occupied adsorbate orbitals and vacant orbitals on the surface [48]. Besides, the distortion of the surface on the Pt–Sn alloys is more serious than on the Pt (1 1 1) [23]. And the E_{inter} decreases with the increasing concentration of Sn. Thus, the role of Sn is weakening the interaction between the molecule and the surfaces.

4. Reaction pathways

For the case of 1,3-cyclohexadiene, the scission of the first hydrogen leads to cyclohexadienyl and the scission of the second one leads to benzene, further dehydrogenations produce the phenyl C_6H_5, benzyne C_6H_4, and so on. The 1,3-cyclohexadiene, cyclohexadienyl, and benzene are adsorbed parallel to the surface. However, phenyl, benzyne, and other dehydrogenation products stand upright on Pt (1 1 1) [29] and Pt–Sn alloys. In this section, we discuss the first three 1,3-cyclohexadiene dehydrogenation steps.

4.1. Dehydrogenation of 1,3-cyclohexadiene on the Pt (1 1 1)

The activation energies have been calculated for the amount of carefully selected reaction steps to evaluate the presence of a dominant reaction pathway. The location of a TS is computationally rather demanding, thus only the most stable and the second most stable adsorption configurations of the species involved in the dehydrogenation are used to search for TS. Fig. 7A shows possible reaction pathways for 1,3-cyclohexadiene dehydrogenation on the Pt (1 1 1). The dominant reaction pathway is indicated in bold. If one of the activation energies is significantly lower than the others, this pathway may likely be considered the dominant reaction pathway. Take the first dehydrogenation step as an example, the difference in activation energy of dehydrogenation beginning at fcc-site adsorbed 1,3-cyclohexadiene (TS 1 shown in Fig. 7) and bri-site adsorbed 1,3-cyclohexadiene (TS 3), 0.31 eV, is sufficient to consider the pathway of dehydrogenation of the bri-site adsorbed 1,3-cyclohexadiene as the dominant reaction pathway. And the dehydrogenation barrier of this step is 0.62 eV. This value is within the experimental range 0.52–0.72 eV [2,11].

Four possible pathways are distinguished for the second dehydrogenation step, starting from cyclohexadienyl adsorbed at hcp- and fcc-site. According to the above analysis, the hcp-site cyclohexadienyl is the specie formed via the dominant reaction path. Therefore, two pathways stating from the hcp-site cyclohexadienyl are considered. Activation energies of 0.87 (the bri-site benzene as the production) and 1.35 eV (the fcc-site benzene as the production) are calculated for the second dehydrogenation step. The pathway with the bri-site benzene as the production is the dominant

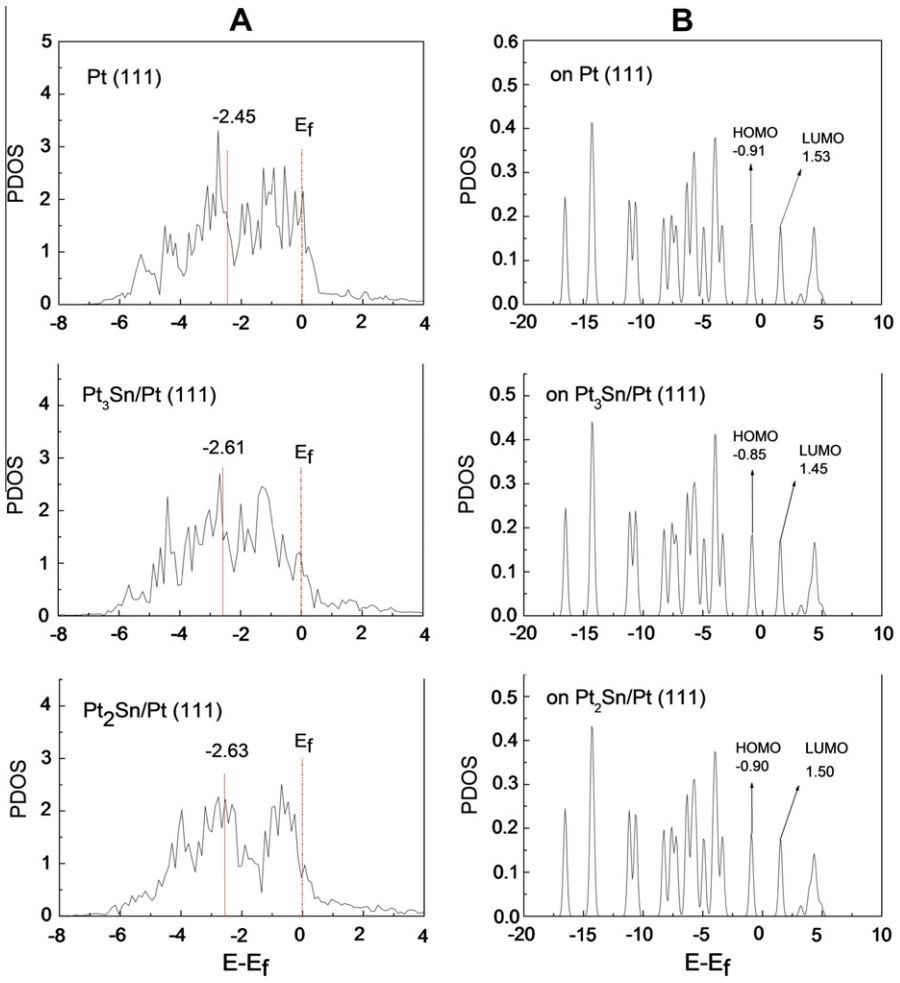

Fig. 6. (A) PDOS projected on the surface Pt atom in the case of Pt (1 1 1), of the Pt_3Sn/Pt (1 1 1) alloy ((4 × 4) cell), and of the Pt_2Sn/Pt (1 1 1) alloy, the dashed line indicates the Fermi level and the vertical segment shows the energy center of the d-band. (B) PDOS of the 1,3-cyclohexdiene adsorbed in the di-π configuration on the Pt(1 1 1), Pt-Sn surfaces.

pathway. And the barrier of 0.87 eV is in accordance with Saeys et al. [4]'s results. Moreover, we also estimate the barrier of diffusion from the most stable adsorption site to the less stable adsorption site (as seen in Fig. 7A), and these diffusion barriers are generally smaller than the reaction barriers, means the possibility of the reaction from the less stable site.

Further dehydrogenation of benzene on Pt (1 1 1) had been investigated by Gao et al. [29], and the dehydrogenation barriers of the bri- and fcc-site adsorbed benzene were calculated to be 1.72 and 1.65 eV with the reaction energy of 0.96 and 0.50 eV. But in our study, they are 1.49 and 1.32 eV with the reaction energy of 0.90 and 0.55 eV. In Peck and Koel [11]'s study, TPD spectra for H_2 on Pt (1 1 1) showed two desorption states at 0.25 ML 1,3-cyclohexadiene coverage: one state at 315 K which was attributed to 1,3-cyclohexadiene dehydrogenation and another at 525 K assigned to benzene decomposition. The temperature required for benzene dehydrogenation is much higher than that for 1,3-cyclohexadiene dehydrogenation. This is consistent with our calculated results: the activation energy of benzene dehydrogenation is more than that of 1,3-cyclohexadiene dehydrogenation (1.49 vs. 0.62 eV).

4.2. Dehydrogenation of 1,3-cyclohexadiene on p (2 × 2) Pt_3Sn/Pt (1 1 1) surface alloy

The dehydrogenation of the less strongly bound hcp-site 1,3-cyclohexadiene has a lower activation energy of 0.72 eV and a reaction energy of 0.20 eV on the Pt_3Sn/Pt (1 1 1). Because of the 0.49 eV lower barrier, the weakly adsorbed hcp-site 1,3-cyclohexadiene is more likely to be the reactive species, whereas the fcc-site species may be too strongly adsorbed and can thus be considered as a spectator species. The second dehydrogenation step prefers to begin at the hcp-site cyclohexadienyl, because the hcp-site cyclohexadienyl is produced by the hcp-site 1,3-cyclohexadiene and it dehydrogenates to benzene with lower barrier of 0.51 eV. The benzene prefers to physisorbed on the Pt_3Sn/Pt (1 1 1) surface. And the barrier for the benzene dehydrogenation to phenyl is 1.75 eV, indicating that this step is dynamically prohibited on the Pt_3Sn/Pt (1 1 1). Therefore, the benzene once produced could desorb from the alloy easily. This is justified by the experimental results [11], TPD showed H_2 evolution from the Pt_3Sn/Pt (1 1 1) alloy surface with a single peak at 340 K at 0.25 ML 1,3-cyclohexadiene coverage, and there was no H_2 desorption at any coverage above 400 K, implying the pathway for benzene dehydrogenation was cut down on the Pt_3Sn/Pt (1 1 1). As a result, the Pt_3Sn/Pt (1 1 1) alloy surface largely increases the selectivity for gas benzene product. And the Sn atom is responsible for the high selectivity on the Pt_3Sn/Pt (1 1 1), because it alters the barrier for 1,3-cyclohexadiene dehydrogenation. In fact, the Pt_3Sn/Pt (1 1 1) alloy had exhibited its high selectivity for 1,3-butadiene hydrogenation to liberate butane at high hydrogen precoverage [9]. And Vigné et al. [10] contributed this high selectivity to the dual role of Sn as site blocking and ligand effect by periodic DFT calculations.

4.3. Dehydrogenation of 1,3-cyclohexadiene on ($\sqrt{3} \times \sqrt{3}$) R30° Pt_2Sn/Pt (1 1 1) surface alloy

The Pt_2Sn/Pt (1 1 1) surface alloy showed the highest selectivity for producing gas benzene in Peck and Koel [11]'s experiment. Based on our theoretical study, this high selectivity of Pt_2Sn/Pt (1 1 1) could be explained as follows: on the one hand, the Pt_2Sn/Pt (1 1 1) surface alloy is much effective in promoting the second dehydrogenation step that produces benzene, as a result of the low dehydrogenation barrier of 0.32 eV. On the other hand, it is difficult for the benzene to dehydrogenate on the Pt_2Sn/Pt (1 1 1), owing to the high dehydrogenation barrier of 1.90 eV. Thus, the major production of 1,3-cyclohexadiene dehydrogenation on Pt_2Sn/Pt (1 1 1) is benzene in gas phase. Besides, the excellent selectivity

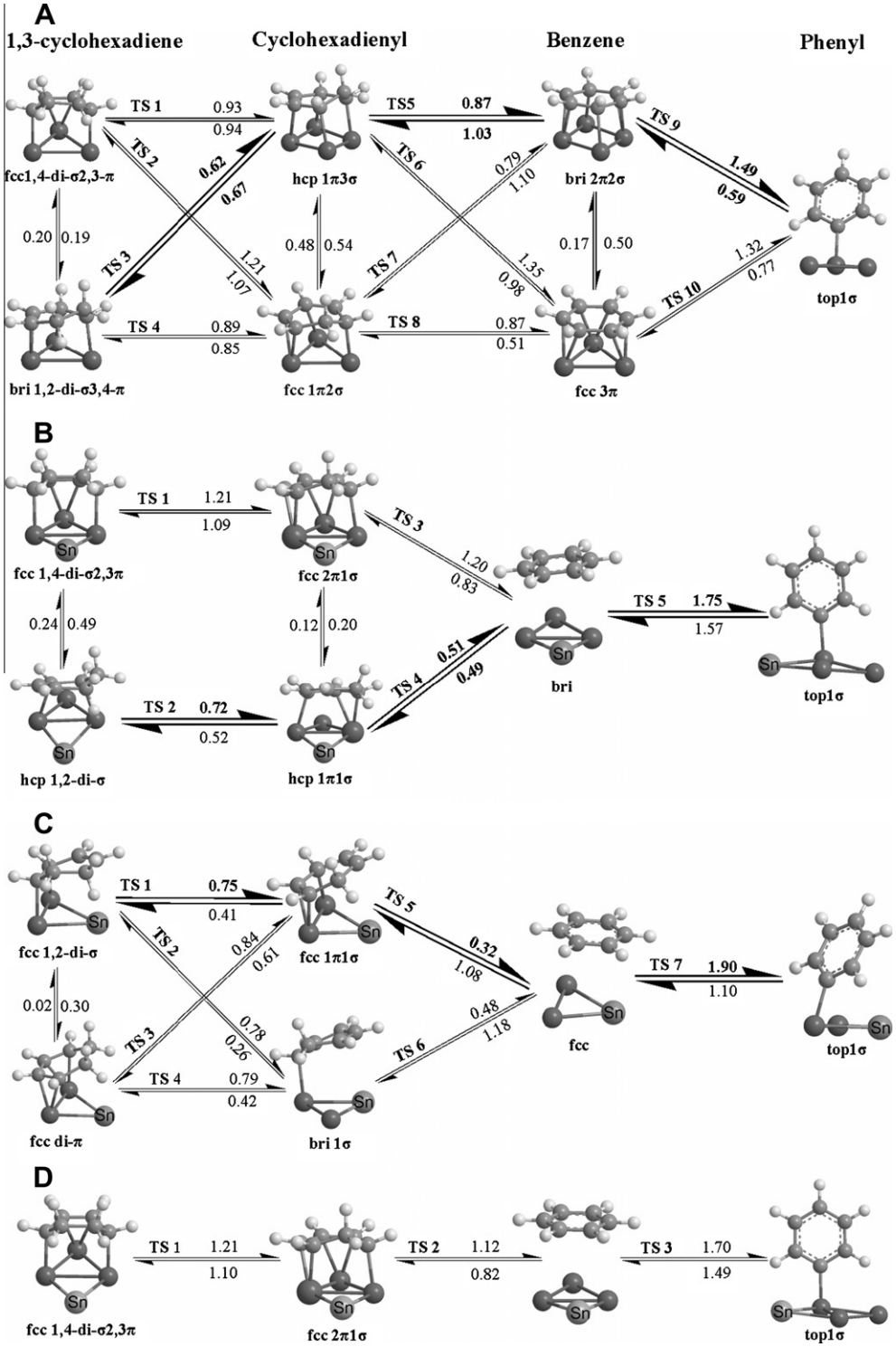

Fig. 7. Possible reaction paths for the dehydrogenation of 1,3-cyclohexadiene on Pt (1 1 1) (A), Pt_3Sn/Pt (1 1 1) ((4 × 4) cell) (B), Pt_2Sn/Pt (1 1 1) (C), and Pt_3Sn/Pt (1 1 1) ((2$\sqrt{3}$ × 2$\sqrt{3}$) cell) (D). The dominant reaction path is indicated in bold. The calculated hydrogenation, dehydrogenation activation energies, and diffusion barriers are indicated. The energy values are given in eV.

of the Pt_2Sn/Pt (1 1 1) alloy surface may be ascribed to the appropriate concentration of Sn, as benzene evolution has been observed to undergo a stepwise decrease in temperature with increasing Sn concentration in the experiments [11].

The elementary steps and TS structures for 1,3-cyclohexadiene dehydrogenation on the Pt–Sn alloys and Pt (1 1 1) are similar (shown in Figs. 7 and 8). The reaction processes can be described as follows: at the beginning of dehydrogenation, the dissociating

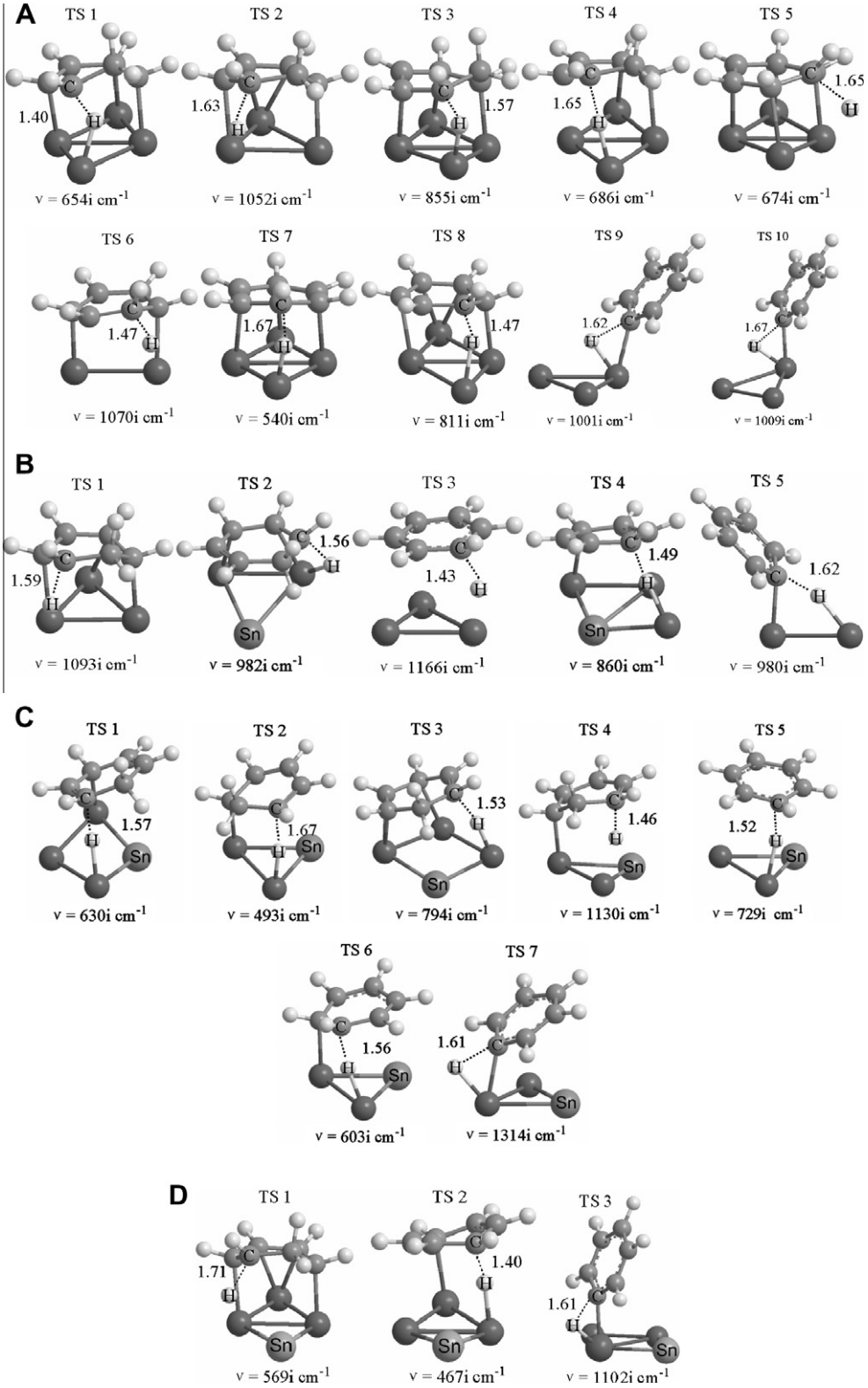

Fig. 8. The structure of all the TS of the three elemental dehydrogenation steps on Pt (1 1 1) (A), Pt_3Sn/Pt (1 1 1) ((4 × 4) cell) (B), Pt_2Sn/Pt (1 1 1) (C), and Pt_3Sn/Pt (1 1 1) ($(2\sqrt{3} \times 2\sqrt{3})$ cell) (D). The dissociative C–H distances (Å) are also labeled.

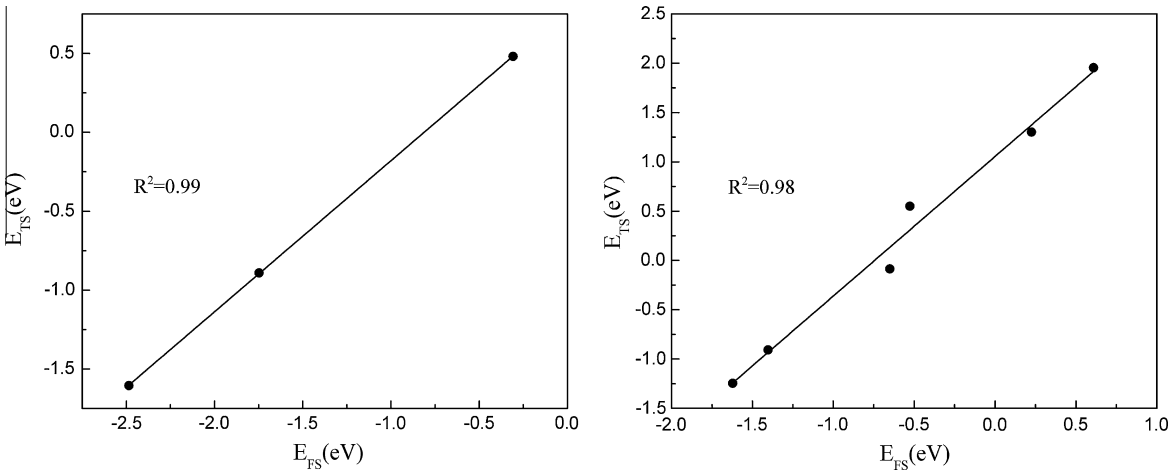

Fig. 9. BEP correlation for C–H bond-breaking steps in 1,3-cyclohexadiene dehydrogenation to phenyl C_6H_5 on the Pt (1 1 1) (the left one) and Pt–Sn surface alloys (the right one). The fit line is $E_{TS}(eV) = 0.96E_{FS} + 0.78$ ($R^2 = 0.99$) for Pt (1 1 1) and $E_{TS}(eV) = 1.42E_{FS} + 1.05$ ($R^2 = 0.98$) for Pt–Sn alloys, where E_{FS} is the energy of the final state for the dominant dehydrogenation reaction, relative to the initial state gas-phase species and the clean slab, E_{TS} is the energy of the corresponding TS with the same reference.

hydrogen atom moves away from the remainder and it begins to localize electron density at the nearest surface Pt atom. The dissociating C–H bond is elongated to be in the range of 1.40–1.71 Å at the TS (see Fig. 8). Then, a new Pt–H bond is formed via the dissociating H and the surface Pt atom after the C–H bond scission.

Furthermore, all the TSs we have studied are more product like, so they can be called "later barrier". There is a good linear relationship between the TS energy and the FS energy (Fig. 9) [50]. It is accepted that BEP (Brønsted–Evans–Polanyi) relationships may apply to reactions in heterogeneous catalysis. And considerable evidence is provided from the experiments [51,52] and theoretical studies [53,54]. However, the classical BEP principle does not work all the time [55,56]. No linear relationship between the activation energy and the reaction energy change is found in our work.

5. Energy decomposition of the reaction barrier

In order to obtain the determined factors for the changes of the barriers, we decompose the calculated barrier (E_{act}) using the following formula: [57]

$$E_{act} = \Delta E_{sub} + \Delta E_{AB}^{def} - E_{AB}^{IS} + E_A^{TS} + E_B^{TS} + E_{A\cdots B}^{int}, \quad (2)$$

where $\Delta E_{sub} = E_{sub}^{TS} - E_{sub}^{IS}$, and reflects the influence of the structural change of the substrate from the initial state (IS) to TS on the activation energy. $\Delta E_{AB}^{def} = E_{A\cdots B}^{gas} - E_{AB}^{gas}$, and is named as deformation energy, which measures the effect of the structural deformation of AB on the barrier. E_{AB}^{IS} is the adsorption energy of AB in the IS configuration. The E_A^{TS} and E_B^{TS} mean the binding energies of A (without B) and B (without A) with the surface in the TS structure and are calculated as $E_{A(B)}^{TS} = E_{A(B)/M} - E_{A(B)} - E_M$, where $_{A(B)}$ means adsorbate, $_M$ means substrate, $_{A(B)/M}$ means the system of A(B) adsorbed on M at the TS. Because all of the TSs, we studied are late TSs, E_A^{TS} and E_B^{TS} reflect largely the A and B bonding ability on the metal surface. It is thus expected that $E_A^{TS} + E_B^{TS}$ is by and large determined by the local electronic effect of metals. The $E_{A\cdots B}^{int}$ is the interaction between A and B in the TS configuration, including bonding competition which is caused by A and B sharing bonding with the same surface atom [57–59] and the direct Pauli repulsion between A and B. Thus, $E_{A\cdots B}^{int}$ is a quantitative measure of the geometrical effect on catalytic reactions. $E_A^{TS} + E_B^{TS}$ and $E_{A\cdots B}^{int}$ are closely related to the TS structure [60]. A denotes C_6H_7, B denotes H for the first C–H bond breaking and the rest can be done in the same manner. Each term of the contributions to the barrier is shown in Table 2.

For the first C–H scission on the Pt (1 1 1) and Pt–Sn surface alloys, ΔE_{sub}, ΔE_{AB}^{def}, $-E_{AB}^{IS}$, and the geometrical effect ($E_{A\cdots B}^{int}$) contribute positively to the barrier. The local electronic effect ($E_A^{TS} + E_B^{TS}$) is much larger than other terms and plays a positive role in reducing the barrier. For the second C–H scission, ΔE_{AB}^{def}, $-E_{AB}^{IS}$, and the geometrical effect ($E_{A\cdots B}^{int}$) share the same trend with the dehydrogenation barrier. A sharp decrease in the local electronic effect ($E_A^{TS} + E_B^{TS}$) and geometrical effect ($E_{A\cdots B}^{int}$) is observed, when compared with the first C–H scission. Besides, the significant reduction in ΔE_{sub} (0.15 eV) and ΔE_{AB}^{def} (−0.53 eV) contribute to the decrease in barrier on the Pt_2Sn/Pt (1 1 1). ΔE_{sub} measures the structural change of the substrate from the IS to the TS. So when the substrate is more relaxed in the TS than in the IS, the value of ΔE_{sub} becomes negative, implying the substrate in the TS is more stable than in the IS. A similar trend that lower activation energy comes with a smaller value of ΔE_{sub} (−0.22 eV) and ΔE_{AB}^{def} (0.67 eV) has also been found for the third C–H scission on Pt (1 1 1). In fact, the local electronic effect ($E_A^{TS} + E_B^{TS}$) plays an important role in reducing the barrier for the third C–H scission. Based on the above analysis, we conclude that the local electronic effect ($E_A^{TS} + E_B^{TS}$) is the crucial factor controlling the barrier for the first and third C–H scission, while the geometrical effect ($E_{A\cdots B^{int}}$) is responsible for the second C–H scission.

6. Microkinetic modeling

A microkinetic model has been developed to investigate the selectivity of the Pt (1 1 1) and Pt–Sn surface alloys for gas-phase benzene production. Table 3 shows the reactions used for the microkinetic modeling and the rate constant at 500 K. Only the forward reactions are taken into consideration. R_1 is assumed in equilibrium. The slowest step is considered as the rds in the present microkinetic model [61]. We have applied the steady-state approximation [62] for the minority species, e.g. C_6H_7, C_6H_6, C_6H_5, and H. Similar kinetic modeling methods have been used for various reactions on metal and metal compound surfaces [62–66]. The equilibrium constant [63,64] is estimated according to $K_{eq} = \exp[-(\Delta E_{ads} - T\Delta S)/k_BT]$, where ΔE_{ads} is the adsorption energy for the adsorbate on the surface, while ΔS is the entropy change of gas-phase adsorbate. The rate constant for R_N ($N = 1, 2, 3, \ldots$) can be described as: $k_N = A\exp(-E_{a,N}/k_BT)$. The pre-exponential factor (A) is considered as a constant (10^{13}) for the sake of simplicity. And we include the zero point energy (ZPE) into the activation

Table 2
Energy decomposition of the calculated activation energy.

	E_{act}	ΔE_{sub}	ΔE_{AB}^{def}	$-E_{AB}^{IS}$	E_A^{TS}	E_B^{TS}	$E_A^{TS}+E_B^{TS}$	$E_{A\cdots B}^{int}$
$C_6H_8 \rightarrow C_6H_7 + H$ ($_A$: C_6H_7 $_B$: H)								
Pt (1 1 1)	0.62	0.12	1.62	1.45	−4.39	−2.67	−7.06	4.48
Pt_3Sn/Pt (1 1 1)	0.72	0.60	0.57	0.67	−2.69	−2.62	−5.31	4.19
Pt_2Sn/Pt (1 1 1)	0.75	0.12	0.62	0.4	−1.26	−2.46	−3.72	3.33
$C_6H_7 \rightarrow C_6H_6 + H$ ($_A$: C_6H_6 $_B$: H)								
Pt (1 1 1)	0.87	0.02	0.86	2.15	−2.49	−2.57	−5.06	2.90
Pt_3Sn/Pt (1 1 1)	0.51	0.26	0.71	1.00	−1.18	−2.43	−3.61	2.15
Pt_2Sn/Pt (1 1 1)	0.32	−0.53	0.15	0.99	−0.09	−2.25	−2.15	1.86
$C_6H_6 \rightarrow C_6H_5 + H$ ($_A$: C_6H_5 $_B$: H)								
Pt (1 1 1)	1.49	−0.22	0.67	0.80	−2.31	−2.60	−4.91	5.14
Pt_3Sn/Pt (1 1 1)	1.75	0.37	2.22	−0.10	−1.76	−2.54	−4.30	3.56
Pt_2Sn/Pt (1 1 1)	1.90	0.43	2.01	−0.06	−1.41	−2.44	−3.85	3.37

Note: B denotes H, A denotes C_6H_7, C_6H_6, C_6H_5 for the first, second, and third dehydrogenation step. E_{act}: the calculated activation energy. ΔE_{sub}: the difference between the energy of the substrate in the transition state and the initial state. ΔE_{AB}^{def}: the difference between the energy of the molecule in the TS and IS. E_{AB}^{IS}: the adsorption energy of the molecule in the IS. E_A^{TS} and E_B^{TS}: the binding energies of A(without B) and B(without A) with the surface in the TS structure. $E_{A\cdots B}^{int}$: the interaction between the dissociated H and the other part of the molecule (unit: eV).

Table 3
The reaction mechanisms and rate constant used for microkinetic modeling on the Pt (1 1 1), Pt_3Sn/Pt (1 1 1), and Pt_2Sn/Pt (1 1 1) surfaces.

Metal surface	Process	E_a (eV)	K $_{eq}$	$k(s^{-1})$
Pt (1 1 1)	R_1 C_6H_8 (gas) + ∗ → C_6H_8∗	–	0.17 (E_{ads} = −1.48 eV[a])	–
	R_2 C_6H_8∗ + ∗ → C_6H_7∗ + H∗	0.52	–	5.7e+8
	R_3 C_6H_7∗ + ∗ → C_6H_6∗ + H∗	0.74	–	3.4e+6
	R_4 C_6H_6∗ → C_6H_6 (gas) + ∗	1.65 [a]	–	2.3e−3
	R_5 C_6H_6∗ + ∗ → C_6H_5∗ + H∗	1.29	–	9.80
	R_6 C_6H_5∗ + ∗ → C_6H_4∗ + H∗	1.21 [a]	–	62.00
	R_7 C_6H_4∗ + ∗ → C_6H_3∗ + H∗	1.43 [a]	–	0.38
	R_8 2H∗ → H_2 (gas) + ∗	0.61	–	7.0e+7
Pt_3Sn/Pt (1 1 1)	R_1 C_6H_8 (gas) + ∗ → C_6H_8∗	–	1.7e−2 (E_{ads} = −1.38 eV[a])	–
	R_2 C_6H_8∗ + ∗ → C_6H_7∗ + H∗	0.67	–	1.7e+7
	R_3 C_6H_7∗ + ∗ → C_6H_6∗ + H∗	0.46	–	2.3e+9
	R_4 C_6H_6∗ → C_6H_6 (gas) + ∗	1.35 [a]	–	2.40
	R_5 C_6H_6∗ + ∗ → C_6H_5∗ + H∗	1.63	–	3.6e−3
	R_6 2C_6H_5 ∗ → $C_{12}H_{10}$ (gas) + 2∗	1.59	–	9.2e−3
	R_7 2H∗ → H_2 (gas) + 2∗	0.40	–	9.2e+9
Pt_2Sn/Pt (1 1 1)	R_1 C_6H_8 (gas) + ∗ → C_6H_8∗	–	1.0e-6 (E_{ads} = −0.96 eV[a])	–
	R_2 C_6H_8∗ + ∗ → C_6H_7∗ + H∗	0.64	–	3.5e+7
	R_3 C_6H_7∗ + ∗ → C_6H_6∗ + H∗	0.23	–	4.8e+11
	R_4 C_6H_6∗ → C_6H_6 (gas) + ∗	0.90 [a]	–	8.4e+4
	R_5 C_6H_6∗ + ∗ → C_6H_5∗ + H∗	1.78	–	1.1e−4
	R_6 2C_6H_5 ∗ → $C_{12}H_{10}$ (gas) + 2∗	1.73	–	3.6e−4
	R_7 2H∗ → H_2 (gas) + 2∗	0.37	–	1.8e+10

Note: An asterisk represents a free site on the surface. The *Keq* is estimated according to $Keq = \exp[-(\Delta Eads - T\Delta S)/kBT]$.The rate constant k is calculated based on $k = A\exp(-Ea/kBT)$.The pre-exponential factor A is considered as a constant (10^{13}). Keq and k are worked out at 500 K. Activation energies are corrected by ZEP corrections. [a] The desorption activation energies of cyclohexdiene and benzene are obtained from literature [11,72], and the reactions of phenyl dehydrogenation are obtained from [69].

energy [67,68] $ZEP = \sum_i (\frac{1}{2})hv_i$, where v_i is the computed real frequencies of the system.

The mechanism for 1,3-cyclohexadiene dehydrogenation to benzene on the Pt (1 1 1) is similar to on the Pt–Sn alloys. But for benzene on the Pt (1 1 1), it was dehydrogenated to leave an adlayer of stoichiometry C_6H_3 around 500 K [69,70]. C_6H_3 was further decomposed to graphitic carbon and hydrogen around 800 K on the Pt (1 1 1) [69,70]. Thus, C_6H_3 can be considered as the end production of C_6H_5 dehydrogenation on the Pt (1 1 1) at 500 K for our microkinetic modeling. Whereas the decomposition of benzene was eliminated on Pt–Sn alloys [11], which is justified by the high calculated dehydrogenation barrier. To be compared with the case on the Pt (1 1 1), di-phenyl ($C_{12}H_{10}$) is considered as the final product on Pt–Sn alloys via the process of dimerization of phenyl (C_6H_5), $2C_6H_5 \rightarrow C_{12}H_{10(g)}$. The dimerization barriers are calculated to be 1.73 eV on the Pt_3Sn/Pt (1 1 1) and 1.88 eV on the Pt_2Sn/Pt (1 1 1) (see Supporting information). So the reactions used for the microkinetic modeling are different on the Pt (1 1 1) from those on the alloys. Moreover, the barrier for hydrogen association to H_2 is calculated to be 0.77 eV on Pt (1 1 1), which is consistent with the results of Grabow et al. [71]. And the association barrier for hydrogen is 0.54 eV on Pt_3Sn/Pt (1 1 1) and 0.50 eV on Pt_2Sn/Pt (1 1 1).

The coverage of surface species (C_6H_8, C_6H_7, C_6H_6) on the Pt (1 1 1) and Pt–Sn alloys can be described below:

$$K_1 = \frac{\theta_{C_6H_8^*}}{P_{C_6H_8}\theta_*}, \quad \theta_{C_6H_8^*} = K_1 P_{C_6H_8}\theta_* \tag{3}$$

$$\frac{d\theta_{C_6H_7^*}}{dt} = k_2\theta_*\theta_{C_6H_8^*} - k_3\theta_*\theta_{C_6H_7^*} = 0, \quad \theta_{C_6H_7^*} = K_1k_2k_3^{-1}P_{C_6H_8}\theta_* \tag{4}$$

$$\frac{d\theta_{C_6H_6^*}}{dt} = k_3\theta_*\theta_{C_6H_7^*} - k_4\theta_{C_6H_6^*} - k_5\theta_*\theta_{C_6H_6^*} = 0, \quad \theta_{C_6H_6^*} = \frac{K_1k_2P_{C_6H_8}}{k_4 + k_5\theta_*}\theta_*^2 \tag{5}$$

The coverage of C_6H_5, C_6H_4 and H on the Pt (1 1 1) is:

$$\frac{d\theta_{C_6H_5^*}}{dt} = k_5\theta_*\theta_{C_6H_6^*} - k_6\theta_*\theta_{C_6H_5^*} = 0, \quad \theta_{C_6H_5^*} = \frac{K_1k_2k_5P_{C_6H_8}}{(k_4 + k_5\theta_*)k_6}\theta_*^2 \tag{6}$$

$$\frac{d\theta_{C_6H_4^*}}{dt} = k_6\theta_*\theta_{C_6H_5^*} - k_7\theta_*\theta_{C_6H_4^*} = 0, \quad \theta_{C_6H_4^*} = \frac{K_1k_2k_5P_{C_6H_8}}{(k_4+k_5\theta_*)k_7}\theta_*^2 \tag{7}$$

$$\frac{d\theta_{H^*}}{dt} = k_2\theta_*\theta_{C_6H_8^*} + k_3\theta_*\theta_{C_6H_7^*} + k_5\theta_*\theta_{C_6H_6^*} + k_6\theta_*\theta_{C_6H_5^*} + k_7\theta_*\theta_{C_6H_4^*} - k_8\theta_{H^*}^2 = 0$$

$$\theta_{H^*} = \sqrt{\frac{(2k_4+5k_5\theta_*)K_1k_2P_{C_6H_8}}{(k_4+k_5\theta_*)k_8}}\theta_* \tag{8}$$

And $$\theta_* + \theta_{C_6H_8^*} + \theta_{C_6H_7^*} + \theta_{C_6H_6^*} + \theta_{C_6H_5^*} + \theta_{C_6H_4^*} + \theta_{C_6H_3^*} + \theta_{H^*} = 1 \tag{9}$$

While the coverage of C_6H_5 and H on the Pt–Sn alloys is:

$$\frac{d\theta_{C_6H_5^*}}{dt} = k_5\theta_*\theta_{C_6H_6^*} - k_6\theta_{C_6H_5^*}^2 = 0, \quad \theta_{C_6H_5^*} = \sqrt{\frac{K_1k_2k_5\theta_*P_{C_6H_8}}{(k_4+k_5\theta_*)k_6}}\theta_* \tag{10}$$

$$\frac{d\theta_{H^*}}{dt} = k_2\theta_*\theta_{C_6H_8^*} + k_3\theta_*\theta_{C_6H_7^*} + k_5\theta_*\theta_{C_6H_6^*} - k_7\theta_{H^*}^2 = 0,$$

$$\theta_{H^*} = \sqrt{\frac{(2k_4+3k_5\theta_*)K_1k_2P_{C_6H_8}}{(k_4+k_5\theta_*)k_7}}\theta_* \tag{11}$$

And $$\theta_* + \theta_{C_6H_8^*} + \theta_{C_6H_7^*} + \theta_{C_6H_6^*} + \theta_{C_6H_5^*} + \theta_{H^*} = 1 \tag{12}$$

By putting the coverage of surface species into Eq. (9) or (12), we can calculate θ_* and other surface converges. Moreover, the rates for the species (C_6H_7, C_6H_6 (gas), C_6H_5, C_6H_3) are: $R_{C_6H_7} = k_2\theta_{C_6H_8^*}\theta_*$, $R_{C_6H_{6(gas)}} = k_4\theta_{C_6H_6^*}$, $R_{C_6H_5} = k_5\theta_{C_6H_6^*}\theta_*$ and $R_{C_6H_3} = k_7\theta_{C_6H_4^*}\theta_*$, respectively. The nonlinear equation was solved using the bisection method.

We are able to roughly estimate the selectivity for gas benzene, on the basis of the above microkinetic model and the DFT-calculated energies. However, the simulated results are not coincided well with the experimental observations [11] if all the DFT results were used directly. We find that there are some differences in the adsorption energies of C_6H_8 and C_6H_6 between our calculated energies and the experiments data [11,72]. So we tried the adsorption energies obtained from experiments (see Table 3) and found they led to more reasonable results: the coverage of empty sites is 0.16 on Pt (1 1 1), 0.26 on Pt_3Sn/Pt (1 1 1) and 1.0 on Pt_2Sn/Pt (1 1 1), and the relative selectivity for gas benzene (ratio of the rate for gas benzene to the total rate for gas benzene and the end production): 0.61 on Pt (1 1 1) $\left(\frac{R_{C_6H_{6(gas)}}}{R_{C_6H_{6(gas)}}+R_{C_6H_3}}\right)$, and 0.99 on Pt_3Sn/Pt (1 1 1) $\left(\frac{R_{C_6H_{6(gas)}}}{R_{C_6H_{6(gas)}}+R_{C_{12}H_{10}}}\right)$ and 1.0 on Pt_2Sn/Pt (1 1 1) $\left(\frac{R_{C_6H_{6(gas)}}}{R_{C_6H_{6(gas)}}+R_{C_{12}H_{10}}}\right)$, under the typical experimental conditions ($P_{C6H8} = 7.4\times10^{-5}$ Pa, $T = 500$ K [11]). This is consistent with the experimental result: the Pt_3Sn/Pt (1 1 1) and Pt_2Sn/Pt (1 1 1) had similar selectivity (nearly 100%) for gas benzene [11], while the Pt (1 1 1) has low selectivity and the competition was strong between desorption and dehydrogenation on Pt (1 1 1) [69]. Fig. 10 shows the temperature dependence of the relative selectivity of gas benzene produced by 1,3-cyclohexadiene dehydrogenation on Pt (1 1 1) and Pt_2Sn/Pt (1 1 1). The relative selectivity for gas benzene decreases sharply from 450 to 580 K on Pt (1 1 1), whereas the relative selectivity for gas benzene remains the same value (nearly 100%) on Pt_2Sn/Pt (1 1 1). In fact, the temperature dependence of selectivity on Pt_3Sn/Pt (1 1 1) is nearly the same as on Pt_2Sn/Pt (1 1 1), and we do not show this result in Fig. 10. So we hold that both the Pt_3Sn/Pt (1 1 1) and the Pt_2Sn/Pt (1 1 1) surface alloys may be an ideal catalyst for promoting 1,3-cyclohexadiene dehydrogenation to gas-phase benzene. This is in agreement well with the experimental observations that the selectivity of benzene formation researched to 100% when the Sn coverage is larger than 0.20 ML [11].

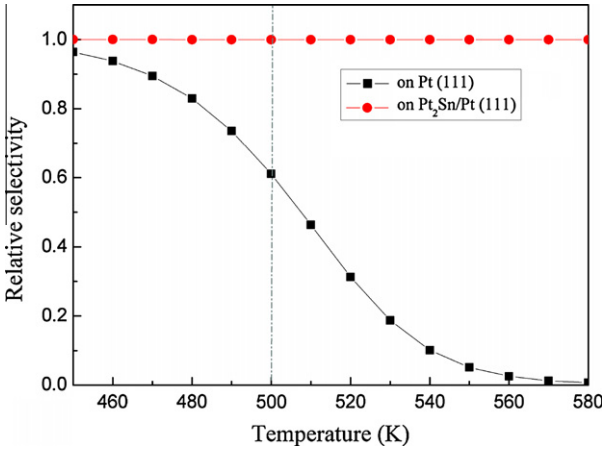

Fig. 10. Temperature dependence of the relative selectivity of gas benzene produced by the 1,3-cyclohexadiene dehydrogenation on Pt (1 1 1) and Pt_2Sn/Pt (1 1 1) using the microkinetic modeling technique ($P_{C6H8} = 7.4\times10^{-5}$ Pa). The dashed line denotes a typical temperature at 500 K.

7. Conclusions

The adsorption of the stable intermediates for 1,3-cyclohexadiene dehydrogenation to phenyl C_6H_5 on the Pt (1 1 1), Pt_3Sn/Pt (1 1 1), and Pt_2Sn/Pt (1 1 1) surface alloys has been explored with periodic DFT–GGA calculations. The calculations exhibit that the interaction between 1,3-cyclohexadiene, cyclohexadienyl, benzene, phenyl, hydrogen atom and the metal surface decreases in the order of Pt (1 1 1) > Pt_3Sn/Pt (1 1 1) > Pt_2Sn/Pt (1 1 1). The d-band center and the work function of the clean Pt (1 1 1), Pt_3Sn/Pt (1 1 1), and Pt_2Sn/Pt (1 1 1) also decrease with the increasing concentration of Sn. The surface Sn atoms increase the repulsion between the adsorbate and the alloy surface, thus weaken the molecule adsorption.

The pathways and activation energies for the 1,3-cyclohexadiene dehydrogenation to phenyl on the Pt (1 1 1), Pt_3Sn/Pt (1 1 1), and Pt_2Sn/Pt (1 1 1) surface alloys have been studied to understand why the alloys have a high selectivity for gas benzene production. Along the dominant reaction path, the barriers on the Pt (1 1 1) are 0.62, 0.87 and 1.49 eV for the first, second, and third dehydrogenation step, respectively. They are 0.72, 0.51, 1.75 eV on the Pt_3Sn/Pt (1 1 1), and 0.75, 0.32, 1.90 eV on the Pt_2Sn/Pt (1 1 1). The rate determined step is the third dehydrogenation step on the three surfaces. The Pt_2Sn/Pt (1 1 1) surface alloy is less active in promoting the first C–H scission step compared with Pt (1 1 1), but it facilitates the second C–H scission step and prohibits further dehydrogenation of benzene. Thus, it is an excellent catalysis for accelerating 1,3-cyclohexadiene dehydrogenation to gas benzene. However, the Pt (1 1 1) is too reactive and therefore no selectivity in the dehydrogenation of 1,3-cyclohexadiene, and the coking product obtained from benzene decomposition could poison the Pt catalyst [69,70]. We suggest the effect of surface Sn concentration on dehydrogenation activity may play an important role in improving the performance of supported Pt–Sn reforming catalysts, and the selectivity researched to 0.99 when the Sn coverage larger than 0.25 ML based on the microkinetic model analysis.

Acknowledgments

This work was supported by the National Natural Science Foundation of China (Grants Nos. 20273034 and 20673063) and the TianHe-1 supercomputer.

Appendix A. Supplementary data

Supplementary data associated with this article can be found, in the online version, at doi:10.1016/j.jcat.2011.04.002.

References

[1] C.L. Pettiette-Hall, D.P. Land, R.T. McIver, J.C. Hemminger, J. Am. Chem. Soc. 113 (1991) 2755.
[2] M.B. Hugenschmidt, A.L. Diaz, C.T. Campbell, J. Phys. Chem. 96 (1992) 5974.
[3] B.E. Koel, D.A. Blank, E.A. Carter, J. Mol. Catal. A: Chem. 131 (1998) 39.
[4] M. Saeys, M.F. Reyniers, M. Neurock, G.B. Marin, J. Phys. Chem. B 107 (2003) 3844.
[5] M. Saeys, M.F. Reyniers, G.B. Marin, M. Neurock, Surf. Sci. 600 (2006) 3121.
[6] C. Morin, D. Simon, P. Sautet, Surf. Sci. 600 (2006) 1339.
[7] S.T. Qi, W.T. Yu, W.W. Lonergan, B. Yang, J.G. Chen, Chin. J. Catal. 31 (2010) 955.
[8] A. Olivas, D.I. Jerdev, B.E. Koel, J. Catal. 222 (2004) 285.
[9] H. Zhao, B.E. Koel, J. Catal. 234 (2005) 24.
[10] F. Vigné, J. Haubrich, D. Loffreda, P. Sautet, F. Delbecq, J. Catal. 275 (2010) 129.
[11] J.W. Peck, B.E. Koel, J. Am. Chem. Soc. 118 (1996) 2708.
[12] F. Delbecq, F. Vigne-Maeder, C. Becker, J. Breitbach, K. Wandelt, J. Phys. Chem. C 112 (2008) 555.
[13] G. Kresse, J. Hafner, Phys. Rev. B 47 (1993) 558.
[14] G. Kresse, J. Hafner, Phys. Rev. B 48 (1993) 13115.
[15] G. Kresse, J. Hafner, Phys. Rev. B 49 (1994) 14251.
[16] G. Kresse, J. Hafner, Phys. Rev. B 59 (1998) 1758.
[17] J.P. Perdew, Y. Wang, Phys. Rev. B 45 (1992) 13244.
[18] M.T. Paffett, S.C. Gebhard, R.G. Windham, B.E. Koel, Surf. Sci. 223 (1989) 449.
[19] G. Henkelman, B. Uberuaga, H. Jonsson, J. Chem. Phys. 113 (2000) 9901.
[20] P. Papon, J. Leblond, P.H.E. Meijer, Phys. Phase Transitions: Concepts Appl. (2006) 91.
[21] J. Haubrich, D. Loffreda, F. Delbecq, P. Sautet, Y. Jugnet, A. Krupski, C. Becker, K. Wandelt, J. Phys. Chem. C 112 (2008) 3701.
[22] A. Atrei, U. Bardi, J.X. Wu, E. Zanazzi, G. Rovida, Surf. Sci. 290 (1993) 286.
[23] C. Becker, J. Haubrich, K. Wandelt, F. Delbecq, D. Loffreda, P. Sautet, J. Phys. Chem. C Lett. 112 (2008) 14693.
[24] J.M. Essen, J. Haubrich, C. Becker, K. Wandelt, Surf. Sci. 601 (2007) 3472.
[25] F. Delbecq, P. Sautet, J. Catal. 220 (2003) 115.
[26] H. Zhao, J. Kim, B.E. Koel, Surf. Sci. 538 (2003) 147.
[27] C. Becker, F. Delbecq, J. Breitbach, G. Hamm, D. Franke, F. Jäger, K. Wandelt, J. Phys. Chem. B 108 (2004) 18960.
[28] C. Xu, Y.L. Tsai, B.E. Koel, J. Phys. Chem. 98 (1994) 585.
[29] W. Gao, W.T. Zheng, Q. Jiang, J. Chem. Phys. 129 (2008) 164705.
[30] G.W. Watson, R.P.K. Wells, D.J. Willock, G. Hutchings, Chem. Commun. 8 (2000) 705.
[31] R.A. Olsen, G.J. Kroes, E.J. Baerends, J. Chem. Phys. 111 (1999) 11155.
[32] R.W. McCabe, L.D. Schmidt, Surf. Sci. 65 (1977) 189.
[33] P.R. Norton, J.A. Davies, T.E. Jackman, Surf. Sci. 121 (1982) 103.
[34] S.C. Gebhard, B.E. Koel, J. Phys. Chem. 96 (1992) 7056.
[35] K. Nobuhara, H. Nahanishi, H. Kasai, A. Okiji, Surf. Sci. 493 (2001) 271.
[36] A.P. Graham, A. Menzel, J.P. Toennies, J. Chem. Phys. 111 (1999) 1676.
[37] C.J. Fall, N. Binggeli, A. Baldereschi, J. Phys.: Condens. Matter 11 (1999) 2689.
[38] M.T. Paffett, S.C. Gebhard, R.G. Windham, B.E. Koel, J. Phys. Chem. 94 (1990) 6831.
[39] P.Q. Yuan, B.Q. Wang, Y.M. Ma, H.M. He, Z.M. Cheng, W.K. Yuan, J. Mol. Catal. A: Chem. 301 (2009) 140.
[40] W. G Xu, Z. F Shang, G.C. Wang, J. Mol. Struct. (Theochem) 869 (2008) 47.
[41] B. Hammer, J.K. Norskov, Surf. Sci. 343 (1995) 211.
[42] M. Mavrikakis, B. Hammer, J.K. Nørskov, Phys. Rev. Lett. 81 (1998) 2819.
[43] P. Kratzer, B. Hammer, J.K. Nørskov, J. Chem. Phys. 105 (1996) 5595.
[44] P. Kratzer, B. Hammer, J.K. Nørskov, Surf. Sci. 359 (1996) 45.
[45] B. Hammer, Y. Morikawa, J.K. Nørskov, Phys. Rev. Lett. 76 (1996) 2141.
[46] F. Delbecq, F. Vigné, J. Phys. Chem. B 109 (2005) 10797.
[47] G. Santarossa, M. Iannuzzi, A. Vargas, A. Baiker, Chem. Phys. Chem. 9 (2008) 401.
[48] C. Morin, D. Simon, P. Sautet, J. Phys. Chem. B 108 (2004) 5653.
[49] C. Morin, D. Simon, P. Sautet, J. Phys. Chem. B 108 (2004) 12084.
[50] T.R. Munter, T. Bligaard, C.H. Christensen, J.K. Nørskov, Phys. Chem. Chem. Phys. 10 (2008) 5202.
[51] M. Kraus, Adv. Catal. 17 (1967) 75.
[52] A.J. Gellman, Q. Dai, J. Am. Chem. Soc. 115 (1993) 714.
[53] V. Pallassana, M. Neurock, J. Catal. 191 (2000) 301.
[54] A. Michaelides, Z.P. Liu, C.J. Zhang, A. Alavi, D.A. King, P. Hu, J. Am. Chem. Soc. 125 (2003) 3704.
[55] D. Loffreda, F. Delbecq, F. Vigné, P. Sautet, Angew. Chem. Int. Ed. 48 (2009) 8978.
[56] S.C. Huang, C.H. Lin, J.H. Wang, J. Phys. Chem. C 114 (2010) 9826.
[57] Z.P. Liu, P. Hu, J. Chem. Phys. 114 (2001) 8244.
[58] Z.P. Liu, P. Hu, J. Am. Chem. Soc. 123 (2001) 12596.
[59] K. Bleakley, P. Hu, J. Am. Chem. Soc. 121 (1999) 7644.
[60] J.J. Mortensen, B. Hammer, J.K. Norskov, Surf. Sci. 414 (1998) 315.
[61] C.T. Campbell, J. Catal. 204 (2001) 520.
[62] P. Liu, A. Logadottir, J.K. Nørskov, Electrochim. Acta 48 (2003) 3731.
[63] P. Liu, J.A. Rodriguez, J. Chem. Phys. 126 (2007) 164705.
[64] P. Liu, J.A. Rodriguez, J. Phys. Chem. B 110 (2006) 19418.
[65] G.-M. Monica, L. Nuria, J. Am. Chem. Soc. 130 (2008) 14406.
[66] Y.M. Choi, P. Liu, J. Am. Chem. Soc. 131 (2009) 13054.
[67] D. Lerch, A. Klein, A. Schmidt, S. Müller, L. Hammer, K. Heinz, M. Weinert, Phys. Rev. B 73 (2006) 075430.
[68] W.Y. Huang, W.Z. Lai, D.Q. Xie, Surf. Sci. 602 (2008) 1288.
[69] J.M. Campbell, S. Seimanides, C.T. Campbell, J. Phys. Chem. 93 (1989) 815.
[70] H. Cabibil, H. Ihm, J.M. White, Surf. Sci. 447 (2000) 91.
[71] L.C. Grabow, A.A. Gokhale, S.T. Evans, J.A. Dumesic, M. Mavrikakis, J. Phys. Chem. C 112 (2008) 4608.
[72] H. Ihm, H.M. Ajo, J.M. Gottfried, P. Bera, C.T. Campbell, J. Phys. Chem. B 108 (2004) 14627.